

# Charge Density Wave Hampers Exciton Condensation in 1T-TiSe<sub>2</sub>

Chao Lian,<sup>1</sup> Zulfikhar A. Ali,<sup>1</sup> and Bryan M. Wong<sup>1,\*</sup>

<sup>1</sup>*Department of Chemical & Environmental Engineering,  
Materials Science & Engineering Program, and Department of Physics & Astronomy,  
University of California-Riverside, Riverside, CA 92521, USA.*

(Dated: December 20, 2024)

The Bose-Einstein condensation of excitons continues to garner immense attention as a prototypical example for observing emergent properties from many-body quantum effects. In particular, Titanium Diselenide (TiSe<sub>2</sub>) is a promising candidate for realizing exciton condensation and was experimentally observed only very recently [Science **358** 1314 (2017)]. Surprisingly, the condensate was experimentally characterized by a soft plasmon mode that only exists near the transition temperature,  $T_c$ , of the charge density wave (CDW). Here, we characterize and analyze the experimental spectra using linear-response time-dependent density functional theory and find that the soft mode can be attributed to interband electronic transitions. At the CDW state below  $T_c$ , the periodic lattice distortions hamper the spontaneous formation of the exciton by introducing a CDW gap. Our surprising results contradict previous simplistic analytical models commonly used in the scientific literature. In addition, we find that a finite electronic temperature,  $T_e$ , introduces an effective band gap and prevents the condensation above  $T_c$ . The band gap lifts the soft mode and merges it into the regular intraband plasmon. The combined effect of the CDW and  $T_e$  explains the fragile temperature-dependence of the exciton condensation. Taken together, our work provides the first *ab initio* atomic-level framework for rationalizing recent experiments and further manipulating exciton condensates in TiSe<sub>2</sub>.

## I. INTRODUCTION

Bose-Einstein condensates (BECs) exhibit exotic transport phenomena such as superfluidity in liquid Helium and superconductivity via Cooper pairs. Other bosonic quasiparticles, such as excitons [1–14], polaritons [15–24], and magnons [25–29] can also form a BEC, with exciton condensation particularly drawing immense recent attention [30]. The exciton condensate is predicted to form a superfluid current [31, 32], which not only is an exotic emergent phenomenon in fundamental quantum research, but also vital for designing next-generation, scattering-free electronic devices.

From a Bardeen-Cooper-Schrieffer (BCS)-like Hamiltonian, Kohn, Jérôme, Halperin, and Rice proposed the phenomenon of exciton condensation in the 1960s [33–35]. Simply put, for a material having an indirect gap, excitons spontaneously form if the exciton binding energy  $E_B$  is larger than the band gap,  $E_G$ . Among the materials that meet this bandstructure requirement, TiSe<sub>2</sub> [Fig. 1] is a particularly promising candidate for observing exciton condensation effects [36]. Above the transition temperature  $T_c \sim 190$  K, TiSe<sub>2</sub> has a negative indirect gap, forming an electron pocket at the M point and a hole pocket at the  $\Gamma$  point, as shown in Fig. 1(c). Besides its semimetallic nature, the quasi-two-dimensional (2D) structure of TiSe<sub>2</sub> weakens the Coulomb screening and favors exciton binding. In a pioneering experimental study, Kogar et al. recently observed exciton condensation in TiSe<sub>2</sub> using electron energy loss spectroscopy (EELS) [30]. At  $T_c$ , the exciton condensation emerges as

a soft plasmon mode near the edge of the Brillouin zone (BZ), which indicates that zero energy consumption is required to excite the electrons. In contrast to conventional BEC effects that are always stable at a sufficiently low temperature, the soft mode is fragile to both an increase and decrease of the temperature [30]. As summarized in Fig. 2(a), instead of a sustainable soft plasmon mode, a momentum-independent plasmon and a regular metallic plasmon are observed at 17 and 300 K, respectively. The highly temperature-dependent exciton condensation reflects the rich physics in TiSe<sub>2</sub>. Specifically, the well-known charge density wave (CDW) emerges below  $T_c$ , accompanied with a  $2 \times 2$  periodic lattice distortion (PLD)  $\{\mathbf{d}_i\}$  shown in Fig. 1(a). Although the CDW state has been extensively studied as a prototypical example of the CDW-superconductivity (SC) transition [37–62], the driving force of the CDW is still under debate regarding whether it is a pure electronic exciton-related mechanism [63–89] or an electron-phonon coupling (EPC) mechanism [90–105]. The complex interplay among the thermal field, CDW order, and exciton condensation is beyond existing conventional models based on the assumption of fixed ions and single-particle bands [33–36]. As such, a first-principles-based *ab initio* framework is essential for understanding this entangled system and tuning the properties of the exciton condensation.

In this communication, we accurately reproduce and characterize the experimental spectra using linear-response time-dependent density functional theory (lr-TDDFT). At the normal state, we observe a soft plasmon mode that directly represents the exciton condensation, which can be attributed to interband electronic transitions. At the CDW state below  $T_c$ , the periodic lattice

\* bryan.wong@ucr.edu

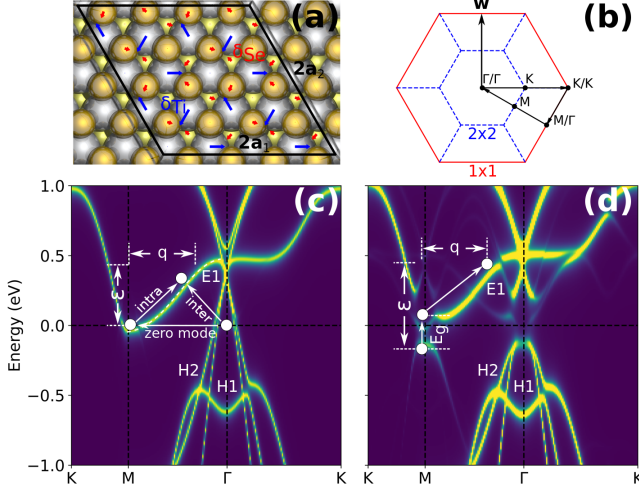


FIG. 1. (a) The structure of 1T-TiSe<sub>2</sub>. The silver, yellow, and orange spheres denote the Ti atoms, the Se atoms on the bottom layer, and the Se atoms on the top layer, respectively. The arrows denote the PLD displacements  $\{\mathbf{d}_i\}$ . The blue and red arrows denote the PLD of the Ti and Se atoms, respectively. (b) The Brillouin zone (BZ) of TiSe<sub>2</sub>. The solid red and dashed blue lines denote the BZ of the  $2 \times 2$  and  $1 \times 1$  TiSe<sub>2</sub> cell, respectively.  $\{\Gamma, M, K\}$  and  $\{\bar{\Gamma}, M, \bar{K}\}$  denote the special  $k$  points in the  $1 \times 1$  and  $2 \times 2$  BZ, respectively. Band structure of 1T-TiSe<sub>2</sub> at (c) the normal state and (d) CDW state.

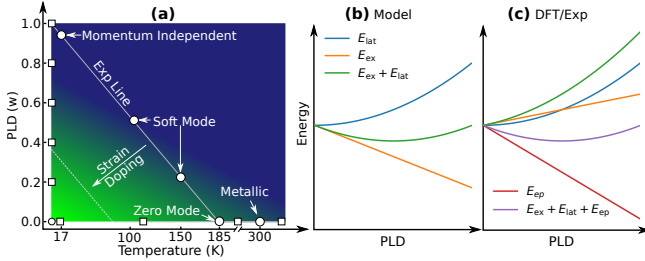


FIG. 2. (a) Phase diagram of TiSe<sub>2</sub>. Green and blue areas denote the exciton condensate and regular phase, respectively. Circles and squares denote the experimental measurements and our simulations. The lattice energy  $E_{\text{lat}}$ , exciton energy  $E_{\text{ex}}$ , electron-phonon energy  $E_{\text{ph}}$ , and total energy  $E_{\text{tot}}$  as a function of the PLD, indicated by (b) the analytical model and (c) our DFT and experimental framework.

distortions introduce a CDW gap and hamper the spontaneous formation of the exciton. Above  $T_c$ , the higher electronic temperature prevents the condensation by introducing an effective band gap. The combined effect of the CDW and finite electronic temperature explains the fragile temperature-dependence of the exciton condensation. Both the CDW and effective band gaps lift the soft mode and merge it into the regular intraband plasmon. Our work provides the first *ab initio* atomic-level framework, beyond widely-used simplistic analytical models, for rationalizing recent experiments and further manipu-

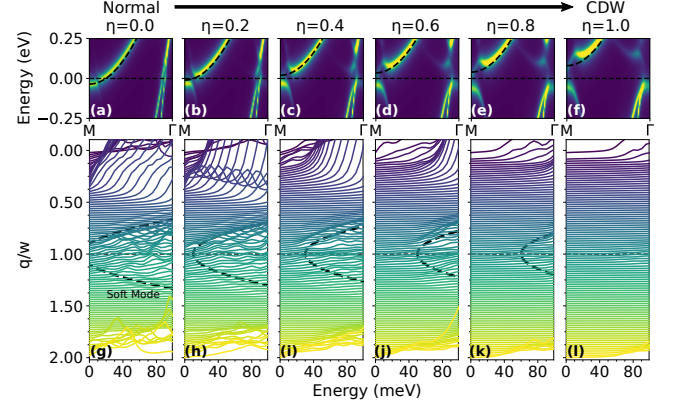


FIG. 3. (a-f) EBS and (g-l) EELS at different PLDs. The dashed lines in panels (a-f) and (g-l) denote the parabolic fittings of the band structures [Eq. 1] near the M point and the plasmon dispersions [Eq. 2] near  $w$ , respectively.

lating exciton condensates in TiSe<sub>2</sub>.

## II. RESULTS AND DISCUSSION

We calculate the structures of the normal  $1 \times 1$  and  $2 \times 2$  CDW phase and obtained the optimized PLD displacements  $\{\mathbf{d}_i\}$  shown in Fig. 1(a), with  $\delta_{Ti} = 0.083 \text{ \AA}$ ,  $\delta_{Se} = 0.027 \text{ \AA}$  and  $\delta_{Ti}/\delta_{Se} = 3.07 : 1$ . These results accurately reproduce the experimental measurements of  $\delta_{Ti} = 0.085 \pm 0.014 \text{ \AA}$  and  $\delta_{Ti}/\delta_{Se} \sim 3 : 1$  [106]. To directly compare with the ARPES measurements, we unfold the energy bands from the  $2 \times 2$  BZ to the  $1 \times 1$  BZ to generate the effective band structures (EBS) [107] along the K-M- $\Gamma$ -K symmetry points, as shown in Fig. 1(b). At the normal state, TiSe<sub>2</sub> is semimetallic [Fig. 1(c)]: the conduction band E1 crosses the Fermi energy near the M point, leading to an electron pocket; a hole pocket appears at  $\Gamma$  surrounded by the two valence bands H1 and H2. At low temperatures, the CDW state of 1T-TiSe<sub>2</sub> is a semiconductor. The  $2 \times 2$  CDW order backfolds the H1 band to the M point. Induced by the avoided crossing, a repulsive force lifts the E1 band and opens a gap of  $E_g \sim 0.1 \text{ eV}$  [Fig. 1(d)]. Via the same mechanism, the backfolded E1 band at the  $\Gamma$  point cuts the H1 and H2 bands into valence and conduction parts and upshifts the conduction parts of the H1 and H2 bands to about 0.1 eV.

Our calculations allow us to build a microscopic framework of the exciton condensation by characterizing the plasmon. As shown in Fig 1(c), when the exciton condensation occurs, electrons near the Fermi level jump from  $\Gamma$  to the M point without an energy cost. This indicates a zero mode in the interband plasmon at the momentum  $q \rightarrow w$  that can be detected by incident electrons exchanging a momentum  $w$  without energy loss. As shown in Fig. 3(g), we observed the zero mode in our EELS simulations. The plasmon energy  $\epsilon(q)$  decreases with  $q < w$ , reaches the zero point  $\epsilon(q) = 0 \text{ eV}$  at  $q = w$  and then increases with  $q > w$ . This behavior is consistent with

TABLE I. Parameters in Eq. [1–3] with different  $\eta$ .

$\eta$	0.0	0.2	0.4	0.6	0.8	1.0
$E_g$ (meV)	-35	0	20	40	50	100
$T_e$ (K)	0	12	117	232	580	1161
$E_c$ (meV)	0	2	20	40	100	200

the experimental observations [30], although the rate of change is higher in our simulation. The experimental energy range of the soft mode is 0–40 meV, whereas we obtain a range of 0–100 meV from our simulations, which is due to the underestimation of the Coulomb screening in DFT [108].

As previously mentioned, the soft mode is highly temperature-dependent and distinguishable from other BEC phenomena. Thus, the knowledge of thermal field effects is essential for understanding the exciton condensation. We propose that the thermal field mainly influences the electronic structures in two aspects: **(I)** The decrease in temperature stabilizes the PLD and introduces a CDW gap. **(II)** The increase in temperature of the electron system  $T_e$  creates more thermal carriers. As shown in Fig. 2(a), both  $T_e$  and PLD cannot be disentangled in the experiment, and only the states on the experimental line can be observed. Nevertheless, our *ab initio* techniques are not limited to these experimentally-observed states and are capable of further sampling the phase diagram and characterizing the effects of the PLD and  $T_e$  separately.

We first examine the effects of the PLD by calculating the EBS and EELS for six structures with different PLDs  $\{\eta\mathbf{d}_i\}$  at  $T_e = 0$  K, where  $\eta = 0.0, 0.2, \dots, 1.0$ , (i.e., the states along the Y axis in Fig 2(a)).  $\eta = 0.0$  and  $\eta = 1.0$  correspond to the normal and CDW state, respectively. The intermediate  $\eta$  values describe the structures at low but finite temperatures  $0 < T < T_c$ . To quantitatively describe the effect of the PLD, we construct an expression for this band-plasmon correspondence. As shown in Fig. 3(a-f), the low energy range band can be accurately described by the expression

$$E(k) = \max\{\alpha(k - k_M)^2 + E_g, 0\}, \quad (1)$$

where  $k_M$  is the  $k$  coordinates of the M point,  $\alpha = 0.95$  eV/Å<sup>2</sup>, and  $E_g$  are the gaps shown in Table I. As shown in Fig. 3(g-l), we find that the interband plasmon dispersion near  $w$  can be accurately described by the expression

$$\epsilon(q) = \max\{\alpha(q - w)^2 + E_g, 0\}, \quad (2)$$

with the same  $\alpha = 0.95$  eV/Å<sup>2</sup> and  $E_g$  values in Eq. 1. This indicates that the incident beam pumps electrons from  $\Gamma$  to the E1 band, producing the EELS signal near  $w$ , as shown in Fig. 3(a). At the normal state, we observed a soft mode with zero excitation energy at  $q = w$ .

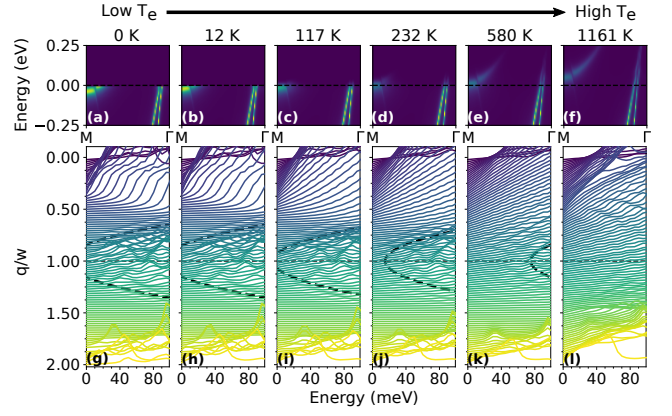


FIG. 4. (a-f) EBS and (g-l) EELS at different electronic temperatures  $T_e$ . The dashed lines in (g)-(l) denote the plasmon dispersions [Eq. 3] near  $w$ .

In addition, the band gap increases with  $\eta$  and consequently lifts the soft mode to a higher energy. The excitation energy at  $q = w$  concomitantly increases from zero to a finite value, preventing the spontaneous exciton condensation.

Next, we discuss the influence of electronic temperature  $T_e$  on the exciton condensation. We simulated the EELS at the normal state with different  $T_e$  values, as shown in Fig. 4. The increase in  $T_e$  changes the electron distribution but barely alters the band structure [Fig. 4(a)-(f)]. Accordingly, the thermal carriers gradually fill the empty bands as  $T_e$  increases. To form the plasmon, the electrons require extra energy,  $E_c$ , to jump into the partially-occupied conduction band due to the repulsion from the thermally-excited carrier. Similar to the CDW gap, the additional  $E_c$  energy lifts the soft mode, as shown in Fig. 4(g)-(l). To account for this effect, we introduce an additional  $E_c$  term into Eq. 2 as

$$\epsilon(q) = \max\{\alpha(q - w)^2 + E_g + E_c, 0\}, \quad (3)$$

where  $E_g = -35$  meV, and  $E_c$  is shown in Table I. From our fitting results, we find that  $E_c$  is proportional to the electronic temperature  $T_e$ .

Combining our analysis of the effects of the PLD and  $T_e$ , we have developed a microscopic framework to explain the temperature dependence of the plasmon dispersion. At a high temperature of  $T = 300$  K, TiSe<sub>2</sub> is semimetallic without a PLD, and the thermal carriers occupy the E1 band and prevent the condensation. At a low temperature of  $T = 17$  K, the thermal excitation is suppressed, while the energy required to create an exciton significantly increases due to the emerging CDW gap. Near the transition temperature at  $T = T_c$ , both the PLD and carrier density are sufficiently small, resulting in the observed zero modes. Thus, we propose that suppressing the PLD at low temperatures can broaden the exciton condensation area, as shown in Fig. 2(a), which can be achieved with compressive strain and charge doping [57, 97, 109, 110].



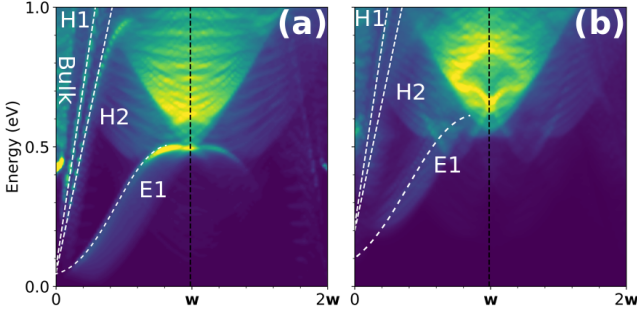


FIG. 5. EELS contour of  $\text{TiSe}_2$  at (a) the normal state and (b) CDW state. The dashed white lines reproduce the bands of E1, H1, and H2 of Fig. 1(c) [Eq. 4] and (d) [Eq. 5], respectively.

The complex effects of the thermal field obtained from our *ab initio* calculations provide a new mechanistic explanation that is quite distinct from the results of the analytical model commonly used in the scientific literature. As shown in Fig. 2(b), the analytical model indicates that the CDW state is a compromise between the increasing lattice energy and the decreasing electron energy via the formation of excitons [98]. This indicates that the exciton condensation distorts the lattice and lowers the energy of the system. Thus, the zero mode should not be destroyed by the PLD, provided that  $T < T_c$ . Instead, both the experimental spectra [30] and our EELS simulation show a different phenomenon: the PLD hinders the exciton condensation, which indicates another mechanism such as EPC is essential for stabilizing the CDW state [Fig. 2(c)].

To complete our story, we discuss the interaction between the interband exciton-like plasmon and the intraband regular plasmon. Similar to other semimetals, the oscillation of the electrons forms gapless plasmons in  $\text{TiSe}_2$ , as shown in Fig. 1(c). At the normal state, four plasmon branches are observed. The energies of the plasmon increase with  $q$ , as shown in Fig. 5(a). Among these branches, a typical bulk plasmon starts from 0.42 eV, while the other three start from zero with different rates. Two of the three branches increase linearly, faster than the other one that resembles a bell shape. At the CDW state, the EELS shows different features: three branches start at a finite energy instead of zero [Fig. 5(b)].

By analyzing the rates quantitatively, we found that one-to-one correspondences exist between the dispersions of the EBS  $E_{\text{band}}^N(k)$  [Fig. 1(c)] and the intraband plasmon  $\epsilon_{\text{band}}^N(q)$  with

$$\begin{aligned}\epsilon_{\text{H1}}^N(q) &= E_{\text{H1}}^N(k_\Gamma \pm q) \\ \epsilon_{\text{H2}}^N(q) &= E_{\text{H2}}^N(k_\Gamma \pm q) \\ \epsilon_{\text{E1}}^N(q) &= E_{\text{E1}}^N(k_M \pm q)\end{aligned}\quad (4)$$

where  $N$  represents the normal state, and  $k_\Gamma$  and  $k_M$  are the reciprocal coordinates of the  $\Gamma$  and  $M$  points, respectively. As shown in Fig. 5(a), the plasmon dis-

persions predicted accurately by Eq. 4 demonstrate the unambiguous intraband nature of the E1, H1, and H2 plasmon branches. Stimulated by the incident beam, the electrons drift along the E1, H1, and H2 bands and form the intraband plasmon, as illustrated in Fig. 1(c), where the plasmon branches are labeled by their contributing bands. For the CDW state, the plasmon can be explained with the same intraband mechanisms with a minor correction: as shown in Fig. 1(d), the electrons still form the plasmon by oscillating along the E1 (H1 and H2) bands, after they are elevated over the band gap that requires an extra energy cost. As shown in Fig. 5(b), the plasmon dispersions are accurately characterized as

$$\epsilon_i^C(q) = \epsilon_i^N(q) + E_g, \quad (5)$$

where  $E_g = 0.1$  eV is the CDW gap, C stands for the CDW state,  $i = \text{E1, H1, and H2}$ , and  $\epsilon_i^N(q)$  is the intraband plasmon dispersion at the normal state from Eq. 4.

The intraband and interband plasmon branches separate in the energy range at low  $T_e$ , and the intraband plasmon branches increase rapidly across the energy range of the interband plasmon ( $< 100$  meV). The increasing  $T_e$  will lift the intraband branch into the intraband region. Since the intraband branches have much stronger intensities, they will dominate the overall EELS signals and recover the normal semi-metallic features of  $\text{TiSe}_2$ .

### III. CONCLUSIONS

In summary, we have developed a new *ab initio* atomic-level framework of the exciton condensation in  $\text{TiSe}_2$ . Our lr-TDDFT approach both accurately reproduces the experimental spectra as well as explains the complex interplay among the thermal field and CDW order effects that were recently observed in exciton condensation experiments. We find that the soft mode that characterizes the exciton condensation can be attributed to interband electronic transitions. Furthermore, the fragile temperature dependence of the exciton condensation is the combined effect of the CDW and thermal carriers: Below  $T_c$ , the periodic lattice distortions hamper the spontaneous formation of the exciton by introducing a CDW gap; above  $T_c$ , a higher electronic temperature produces sufficient thermal carriers and introduce an effective band gap. Both the CDW and effective band gaps lift the soft mode and merge it into the regular intraband plasmon, which explains why the soft mode is only observed at  $T_c$ . As such, our *ab initio* framework provides critical mechanistic insight into recent exciton condensation experiments and presents additional avenues to experimentalists for further manipulating exciton condensates in  $\text{TiSe}_2$ .

#### IV. ACKNOWLEDGEMENT

C. L. acknowledges support from the UC Riverside Collaborative Seed Grant. Z. A. A. and B. M. W. acknowledge financial support from the Office of Naval Research (Grant N00014-18-1-2740).

#### V. METHODOLOGY

The ground state and lr-TDDFT calculations were carried out with the GPAW [111–113] package. The projector augmented-waves (PAW) [114] method and Perdew-Burke-Ernzerhof (PBE) XC functional [115] were used. The plane-wave cutoff energy was set to 750 eV. The Brillouin zone was sampled using the Monkhorst-Pack (MP) scheme [116] with a  $48 \times 48 \times 1$  k-point mesh. The computational cell examined in this work was a  $2 \times 2$  supercell of TiSe<sub>2</sub>, containing 4 Ti atoms and 12 Se atoms. In the lr-TDDFT calculations, the Bootstrap XC kernel [117] was utilized together with the RPA as a comparison.

#### VI. SUPPORTING INFORMATION

We calculate the EELS, i.e. the frequency and wave-vector dependent density response functions, based on the lr-TDDFT formalism [118–120]. The non-interacting density response function in real space is written as

$$\chi^0(\mathbf{r}, \mathbf{r}', \omega) = \sum_{\mathbf{k}, \mathbf{q}} \sum_{n, n'} \frac{f_{n\mathbf{k}} - f_{n'\mathbf{k}+\mathbf{q}}}{\omega + \epsilon_{n\mathbf{k}} - \epsilon_{n'\mathbf{k}+\mathbf{q}} + i\eta} \times \psi_{n\mathbf{k}}^*(\mathbf{r}) \psi_{n'\mathbf{k}+\mathbf{q}}(\mathbf{r}) \psi_{n\mathbf{k}}(\mathbf{r}') \psi_{n'\mathbf{k}+\mathbf{q}}^*(\mathbf{r}'), \quad (6)$$

where  $n$  is the band index,  $\mathbf{k}$  is the  $k$  index,  $\mathbf{q}$  stands for the Bloch vector of the incident wave,  $\eta \rightarrow 0$ , and  $\epsilon_{n\mathbf{k}}$  and  $\psi_{n\mathbf{k}}(\mathbf{r})$  are the eigenvalues and eigenvectors of the ground state Hamiltonian, respectively. The full interacting density response function is obtained by solving Dyson's equation from its non-interacting counterpart  $\chi^0$  as

$$\chi(\mathbf{r}, \mathbf{r}', \omega) = \chi_0(\mathbf{r}, \mathbf{r}', \omega) + \iint_{\Omega} d\mathbf{r}_1 d\mathbf{r}_2 \chi_0(\mathbf{r}, \mathbf{r}_1, \omega) K(\mathbf{r}_1, \mathbf{r}_2) \chi(\mathbf{r}_2, \mathbf{r}', \omega), \quad (7)$$

where the kernel is the summation of the coulomb and exchange-correlation (XC) interaction

$$K(\mathbf{r}_1, \mathbf{r}_2) = \frac{1}{|\mathbf{r}_1 - \mathbf{r}_2|} + f_{xc}. \quad (8)$$

Here,  $f_{xc} = \partial V_{xc}[n]/\partial n$  is the XC kernel. The commonly-used XC kernels include the adiabatic local density approximation (ALDA) [115], Bootstrap approximation [117], etc. One of the simplest cases is the random phase approximation (RPA), with  $f_{xc} = 0$ .

For a system possessing translational symmetry, it is more convenient to represent  $\chi^0$  in the reciprocal lattice space:

$$\chi^0(\mathbf{r}, \mathbf{r}', \omega) = \frac{1}{\Omega} \sum_{\mathbf{q}} \sum_{\mathbf{G}, \mathbf{G}'} e^{i(\mathbf{q}+\mathbf{G})\cdot\mathbf{r}} \chi_{\mathbf{G}\mathbf{G}'}^0(\mathbf{q}, \omega) e^{-i(\mathbf{q}+\mathbf{G}')\cdot\mathbf{r}'}, \quad (9)$$

where  $\Omega$  is the normalization volume and  $\mathbf{G}(\mathbf{G}')$  are reciprocal lattice vectors. The Fourier coefficients  $\chi_{\mathbf{G}\mathbf{G}'}^0(\mathbf{q}, \omega)$  are written as

$$\chi_{\mathbf{G}\mathbf{G}'}^0(\mathbf{q}, \omega) = \sum_{n, n'} \chi_{\mathbf{G}\mathbf{G}'}^0{}_{n, n'}(\mathbf{q}, \omega) \quad (10)$$

where

$$\begin{aligned} \chi_{\mathbf{G}\mathbf{G}'}^0{}_{n, n'}(\mathbf{q}, \omega) = & \frac{1}{\Omega} \sum_{\mathbf{k}} \frac{f_{n\mathbf{k}} - f_{n'\mathbf{k}+\mathbf{q}}}{\omega + \epsilon_{n\mathbf{k}} - \epsilon_{n'\mathbf{k}+\mathbf{q}} + i\eta} \\ & \times \langle \psi_{n\mathbf{k}} | e^{-i(\mathbf{q}+\mathbf{G})\cdot\mathbf{r}} | \psi_{n'\mathbf{k}+\mathbf{q}} \rangle_{\Omega_{\text{cell}}} \\ & \times \langle \psi_{n\mathbf{k}} | e^{i(\mathbf{q}+\mathbf{G}')\cdot\mathbf{r}'} | \psi_{n'\mathbf{k}+\mathbf{q}} \rangle_{\Omega_{\text{cell}}}, \end{aligned} \quad (11)$$

Dyson's equation is expressed in the  $\mathbf{G}$  basis

$$\begin{aligned} \chi_{\mathbf{G}\mathbf{G}'}(\mathbf{q}, \omega) = & \chi_{\mathbf{G}\mathbf{G}'}^0(\mathbf{q}, \omega) \\ & + \sum_{\mathbf{G}_1 \mathbf{G}_2} \chi_{\mathbf{G}\mathbf{G}_1}^0(\mathbf{q}, \omega) K_{\mathbf{G}_1 \mathbf{G}_2}(\mathbf{q}) \chi_{\mathbf{G}_2 \mathbf{G}'}(\mathbf{q}, \omega). \end{aligned} \quad (12)$$

The dielectric function can be expressed with  $\chi_{\mathbf{G}\mathbf{G}'}(\mathbf{q}, \omega)$  as

$$\epsilon_{\mathbf{G}\mathbf{G}'}^{-1}(\mathbf{q}, \omega) = \delta_{\mathbf{G}\mathbf{G}'} - \sum_{\mathbf{G}_1} K_{\mathbf{G}\mathbf{G}_1}(\mathbf{q}) \chi_{\mathbf{G}_1 \mathbf{G}'}(\mathbf{q}, \omega). \quad (13)$$

The macroscopic dielectric function is defined by

$$\epsilon_M(\mathbf{q}, \omega) = \frac{1}{\epsilon_{00}^{-1}(\mathbf{q}, \omega)}, \quad (14)$$

and the electron energy loss spectrum (EELS) is

$$\text{EELS} = -\text{Im} \frac{1}{\epsilon_M(\mathbf{q}, \omega)}. \quad (15)$$

We briefly discuss the accuracy of lr-TDDFT in describing the exciton in TiSe<sub>2</sub>. It is known that semi-local XCs (e.g. PBE) poorly describe long-range Coulomb screening [117], and long-range corrections, such as in the BetheSalpeter equation, are required for improved accuracy. However, the exciton in TiSe<sub>2</sub> is formed by an attractive interaction  $V(\mathbf{w})$  between the electron pocket at the M point and the hole pocket at the  $\Gamma$  point, as shown in Fig. 1(d). Here,  $\mathbf{w} = \pm 0.5\mathbf{b}_1$  is the reciprocal vector and  $\mathbf{b}_1$  ( $i = 1, 2$ ) is the reciprocal lattice vector along the  $i$ th direction, as shown in Fig. 1(c). Thus,  $V(\mathbf{w})$  is a medium-ranged interaction with a characteristic distance of  $1/|\mathbf{w}| = a$ , where  $a = |\mathbf{a}_i|$  and  $\mathbf{a}_i$  is the

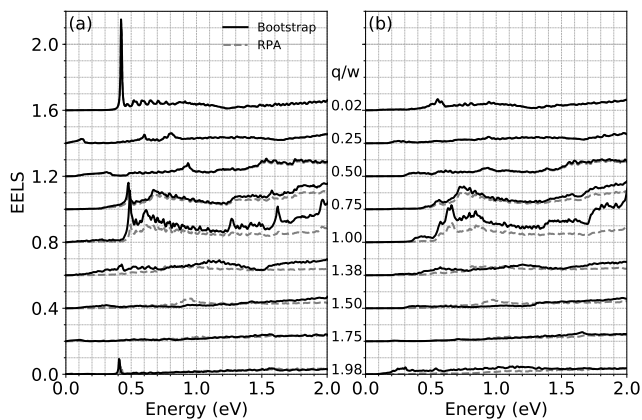


FIG. 6. Comparison of the EELS with RPA vs Bootstrap XC kernels for (a) the normal state (b) the CDW state.

lattice vector.  $V(\mathbf{w})$  is distinctly different from typical long-range interactions that are characteristic of vertical excitonic excitations in momentum space.

We quantitatively characterize the exciton effect by comparing the EELS calculated with the random phase approximation (RPA) and the Bootstrap XC kernel, as shown in Fig. 6. The Bootstrap XC kernel is designed to correct the long-range error of the Coulomb interaction and generates accurate exciton peaks at a similar computational cost of ALDA [117]. At  $q \sim 0$ , the EELS spectra with the RPA and Bootstrap are generally the same, indicating the absence of the exciton-type excitation. We note that with increasing  $q$ , the difference increases and reaches a maximum at  $q = \mathbf{w}$ , corresponding to the emergence of exciton excitations. With a further increase of  $q$ , the RPA and Bootstrap curves overlap with minor shifts in the peaks.

- [1] D. Snoke and G. M. Kavoulakis, *Rep. Prog. Phys.* **77**, 116501 (2014).
- [2] K. Seki, Y. Wakisaka, T. Kaneko, T. Toriyama, T. Konishi, T. Sudayama, N. L. Saini, M. Arita, H. Namatame, M. Taniguchi, N. Katayama, M. Nohara, H. Takagi, T. Mizokawa, and Y. Ohta, *Phys. Rev. B* **90**, 155116 (2014).
- [3] D. W. Snoke, J. P. Wolfe, and A. Mysyrowicz, *Phys. Rev. B* **41**, 11171 (1990).
- [4] K. Johnsen and G. M. Kavoulakis, *Phys. Rev. Lett.* **86**, 858 (2001).
- [5] D. W. Snoke, J. P. Wolfe, and A. Mysyrowicz, *Phys. Rev. Lett.* **64**, 2543 (1990).
- [6] R. Casella, *Journal of Physics and Chemistry of Solids* **24**, 19 (1963).
- [7] J. L. Lin and J. P. Wolfe, *Phys. Rev. Lett.* **71**, 1222 (1993).
- [8] M. Combescot, O. Betbeder-Matibet, and R. Combescot, *Phys. Rev. Lett.* **99**, 176403 (2007).
- [9] G. M. Kavoulakis and A. Mysyrowicz, *Phys. Rev. B* **61**, 16619 (2000).
- [10] P. Cudazzo, C. Attaccalite, I. V. Tokatly, and A. Rubio, *Phys. Rev. Lett.* **104**, 226804 (2010).
- [11] L. V. Butov, C. W. Lai, A. L. Ivanov, A. C. Gossard, and D. S. Chemla, *Nature* **417**, 47 (2002).
- [12] J. M. Blatt, K. W. Ber, and W. Brandt, *Phys. Rev.* **126**, 1691 (1962).
- [13] J. P. Eisenstein and A. H. MacDonald, *Nature* **432**, 691 (2004).
- [14] A. Mysyrowicz, D. W. Snoke, and J. P. Wolfe, *phys. stat. sol. (b)* **159**, 387 (1990).
- [15] H. Deng, G. Weihs, C. Santori, J. Bloch, and Y. Yamamoto, *Science* **298**, 199 (2002).
- [16] D. Porras, C. Ciuti, J. J. Baumberg, and C. Tejedor, *Phys. Rev. B* **66**, 085304 (2002).
- [17] M. Richard, J. Kasprzak, R. André, R. Romestain, L. S. Dang, G. Malpuech, and A. Kavokin, *Phys. Rev. B* **72**, 201301 (2005).
- [18] F. P. Laussy, I. A. Shelykh, G. Malpuech, and A. Kavokin, *Phys. Rev. B* **73**, 035315 (2006).
- [19] M. Wouters and I. Carusotto, *Phys. Rev. Lett.* **99**, 140402 (2007).
- [20] J. Kasprzak, M. Richard, A. Baas, B. Deveaud, R. André, J.-P. Poizat, and L. S. Dang, *Phys. Rev. Lett.* **100**, 067402 (2008).
- [21] Q.-H. Jin, Y. Yuan, Y.-P. Yang, Q.-M. Qiu, M. Liu, Z.-F. Li, Z.-W. Zhang, and C.-L. Zhang, *Polyhedron* **101**, 56 (2015).
- [22] K. G. Lagoudakis, M. Wouters, M. Richard, A. Baas, I. Carusotto, R. André, L. S. Dang, and B. Deveaud-Plédran, *Nature Phys* **4**, 706 (2008).
- [23] H. Deng, H. Haug, and Y. Yamamoto, *Rev. Mod. Phys.* **82**, 1489 (2010).
- [24] J. Kasprzak, M. Richard, S. Kundermann, A. Baas, P. Jeambrun, J. M. J. Keeling, F. M. Marchetti, M. H. Szymańska, R. André, J. L. Staehli, V. Savona, P. B. Littlewood, B. Deveaud, and L. S. Dang, *Nature* **443**, 409 (2006).
- [25] C. Regg, N. Cavadini, A. Furrer, H.-U. Gdel, K. Krmer, H. Mutka, A. Wildes, K. Habicht, and P. Vorderwisch, *Nature* **423**, 62 (2003).
- [26] T. Radu, H. Wilhelm, V. Yushankhai, D. Kovrizhin, R. Coldea, Z. Tylczynski, T. Lhmann, and F. Steglich, *Phys. Rev. Lett.* **95**, 127202 (2005).
- [27] S. O. Demokritov, V. E. Demidov, O. Dzyapko, G. A. Melkov, A. A. Serga, B. Hillebrands, and A. N. Slavin, *Nature* **443**, 430 (2006).
- [28] T. Nikuni, M. Oshikawa, A. Oosawa, and H. Tanaka, *Phys. Rev. Lett.* **84**, 5868 (2000).
- [29] Y. Tserkovnyak, S. A. Bender, R. A. Duine, and B. Flebus, *Phys. Rev. B* **93**, 100402 (2016).
- [30] A. Kogar, M. S. Rak, S. Vig, A. A. Husain, F. Flicker, Y. I. Joe, L. Venema, G. J. MacDougall, T. C. Chiang, E. Fradkin, J. van Wezel, and P. Abbamonte, *Science* **358**, 1314 (2017).
- [31] E. Hanamura and H. Haug, *Solid State Communications* **15**, 1567 (1974).
- [32] H. Haug and E. Hanamura, *Physical Review B* **11**, 3317 (1975).
- [33] W. Kohn, *Phys. Rev. Lett.* **19**, 439 (1967).

- [34] D. Jérôme, T. M. Rice, and W. Kohn, *Phys. Rev.* **158**, 462 (1967).
- [35] B. I. HALPERIN and T. M. RICE, *Rev. Mod. Phys.* **40**, 755 (1968).
- [36] C. Monney, H. Cercellier, F. Clerc, C. Battaglia, E. F. Schwier, C. Didiot, M. G. Garnier, H. Beck, P. Aebi, H. Berger, L. Forró, and L. Patthey, *Phys. Rev. B* **79**, 045116 (2009).
- [37] X. Y. Cui, H. Negishi, S. G. Titova, K. Shimada, A. Ohnishi, M. Higashiguchi, Y. Miura, S. Hino, A. M. Jahir, A. Titov, H. Bidadí, S. Negishi, H. Namatame, M. Taniguchi, and M. Sasaki, *Phys. Rev. B* **73**, 085111 (2006).
- [38] J. I. Lunine, D. P. O'brien, S. N. Raymond, A. Morbidelli, T. Quinn, and A. L. Graps, *adv sci lett* **4**, 325 (2011).
- [39] G. Li, W. Z. Hu, D. Qian, D. Hsieh, M. Z. Hasan, E. Morosan, R. J. Cava, and N. L. Wang, *Phys. Rev. Lett.* **99**, 027404 (2007).
- [40] S. Y. Li, G. Wu, X. H. Chen, and L. Taillefer, *Phys. Rev. Lett.* **99**, 107001 (2007).
- [41] H. Barath, M. Kim, J. F. Karpus, S. L. Cooper, P. Abbamonte, E. Fradkin, E. Morosan, and R. J. Cava, *Phys. Rev. Lett.* **100**, 106402 (2008).
- [42] A. F. Kusmartseva, B. Sipos, H. Berger, L. Forró, and E. Tutiš, *Phys. Rev. Lett.* **103**, 236401 (2009).
- [43] J. Jeong, J. Jeong, H.-J. Noh, S. B. Kim, and H.-D. Kim, *Physica C: Superconductivity and its Applications* **470**, S648 (2010).
- [44] M. Zaberchik, K. Chashka, L. Patlgan, A. Maniv, C. Baines, P. King, and A. Kanigel, *Phys. Rev. B* **81**, 220505 (2010).
- [45] A. D. Hillier, P. Manuel, D. T. Adroja, J. W. Taylor, A. K. Azad, and J. T. S. Irvine, *Phys. Rev. B* **81**, 092507 (2010).
- [46] N. Giang, Q. Xu, Y. S. Hor, A. J. Williams, S. E. Dutton, H. W. Zandbergen, and R. J. Cava, *Phys. Rev. B* **82**, 024503 (2010).
- [47] E. Morosan, K. E. Wagner, L. L. Zhao, Y. Hor, A. J. Williams, J. Tao, Y. Zhu, and R. J. Cava, *Phys. Rev. B* **81**, 094524 (2010).
- [48] M. Iavarone, R. D. Capua, X. Zhang, M. Gholikhan, S. A. Moore, and G. Karapetrov, *Phys. Rev. B* **85**, 155103 (2012).
- [49] J. Kačmarčík, Z. Pribulová, V. Pal'uchová, P. Szabó, P. Husaníková, G. Karapetrov, and P. Samuely, *Phys. Rev. B* **88**, 020507 (2013).
- [50] P. Husaníková, J. Fedor, J. Dérier, J. Šoltýs, V. Cambel, M. Iavarone, S. J. May, and G. Karapetrov, *Phys. Rev. B* **88**, 174501 (2013).
- [51] R. Ganesh, G. Baskaran, J. van den Brink, and D. V. Efremov, *Phys. Rev. Lett.* **113**, 177001 (2014).
- [52] Y. I. Joe, X. M. Chen, P. Ghaemi, K. D. Finkelstein, G. A. de la Peña, Y. Gan, J. C. T. Lee, S. Yuan, J. Geck, G. J. MacDougall, T. C. Chiang, S. L. Cooper, E. Fradkin, and P. Abbamonte, *Nature Phys* **10**, 421 (2014).
- [53] K. Luna, P. M. Wu, J. S. Chen, E. Morosan, and M. R. Beasley, *Phys. Rev. B* **91**, 094509 (2015).
- [54] T. Das and K. Dolui, *Phys. Rev. B* **91**, 094510 (2015).
- [55] Z. Medvecká, T. Klein, V. Cambel, J. Šoltýs, G. Karapetrov, F. Levy-Bertrand, B. Michon, C. Marcenat, Z. Pribulová, and P. Samuely, *Phys. Rev. B* **93**, 100501 (2016).
- [56] F. Levy-Bertrand, B. Michon, J. Marcus, C. Marcenat, J. Kačmarčík, T. Klein, and H. Cercellier, *Physica C: Superconductivity and its Applications* **523**, 19 (2016).
- [57] M. J. Wei, W. J. Lu, R. C. Xiao, H. Y. Lv, P. Tong, W. H. Song, and Y. P. Sun, *Phys. Rev. B* **96**, 165404 (2017).
- [58] A. Kogar, G. de la Pena, S. Lee, Y. Fang, S.-L. Sun, D. Lioi, G. Karapetrov, K. Finkelstein, J. Ruff, P. Abbamonte, and S. Rosenkranz, *Phys. Rev. Lett.* **118**, 027002 (2017).
- [59] S. Yan, D. Iaiia, E. Morosan, E. Fradkin, P. Abbamonte, and V. Madhavan, *Phys. Rev. Lett.* **118**, 106405 (2017).
- [60] A. Banerjee, A. Garg, and A. Ghosal, *Phys. Rev. B* **98**, 104206 (2018).
- [61] B. Hildebrand, T. Jaouen, M.-L. Mottas, G. Monney, C. Barreateau, E. Giannini, D. Bowler, and P. Aebi, *Phys. Rev. Lett.* **120**, 136404 (2018).
- [62] Q. Yao, D. Shen, C. Wen, C. Hua, L. Zhang, N. Wang, X. Niu, Q. Chen, P. Dudin, Y. Lu, Y. Zheng, X. Chen, X. Wan, and D. Feng, *Phys. Rev. Lett.* **120**, 106401 (2018).
- [63] K. Rossnagel, L. Kipp, and M. Skibowski, *Phys. Rev. B* **65**, 235101 (2002).
- [64] H. Cercellier, C. Monney, F. Clerc, C. Battaglia, L. Despont, M. G. Garnier, H. Beck, P. Aebi, L. Patthey, H. Berger, and L. Forró, *Phys. Rev. Lett.* **99**, 146403 (2007).
- [65] N. Stoffel, F. Lévy, C. Bertoni, and G. Margaritondo, *Solid State Communications* **41**, 53 (1982).
- [66] O. Anderson, R. Mancke, and M. Skibowski, *Phys. Rev. Lett.* **55**, 2188 (1985).
- [67] T. Pillo, J. Hayoz, H. Berger, F. Lévy, L. Schlapbach, and P. Aebi, *Phys. Rev. B* **61**, 16213 (2000).
- [68] T. E. Kidd, T. Miller, M. Y. Chou, and T.-C. Chiang, *Phys. Rev. Lett.* **88**, 226402 (2002).
- [69] C. Monney, E. F. Schwier, M. G. Garnier, N. Mariotti, C. Didiot, H. Beck, P. Aebi, H. Cercellier, J. Marcus, C. Battaglia, H. Berger, and A. N. Titov, *Phys. Rev. B* **81**, 155104 (2010).
- [70] C. Monney, E. F. Schwier, M. G. Garnier, N. Mariotti, C. Didiot, H. Cercellier, J. Marcus, H. Berger, A. N. Titov, H. Beck, and P. Aebi, *New J. Phys.* **12**, 125019 (2010).
- [71] J. van Wezel, P. Nahai-Williamson, and S. S. Saxena, *Europhys. Lett.* **89**, 47004 (2010).
- [72] C. Monney, C. Battaglia, H. Cercellier, P. Aebi, and H. Beck, *Phys. Rev. Lett.* **106**, 106404 (2011).
- [73] M. M. May, C. Brabetz, C. Janowitz, and R. Mancke, *Phys. Rev. Lett.* **107**, 176405 (2011).
- [74] C. Monney, G. Monney, P. Aebi, and H. Beck, *New J. Phys.* **14**, 075026 (2012).
- [75] M. Cazzaniga, H. Cercellier, M. Holzmann, C. Monney, P. Aebi, G. Onida, and V. Olevano, *Phys. Rev. B* **85**, 195111 (2012).
- [76] C. Monney, G. Monney, P. Aebi, and H. Beck, *Phys. Rev. B* **85**, 235150 (2012).
- [77] C. Monney, G. Monney, P. Aebi, and H. Beck, *New J. Phys.* **14**, 075026 (2012).
- [78] B. Zenker, H. Fehske, H. Beck, C. Monney, and A. R. Bishop, *Phys. Rev. B* **88**, 075138 (2013).
- [79] S. Koley, M. S. Laad, N. S. Vidhyadhiraja, and A. Taraphder, *Phys. Rev. B* **90**, 115146 (2014).
- [80] H. Watanabe, K. Seki, and S. Yunoki, *Phys. Rev. B* **91**, 205135 (2015).
- [81] J.-P. Peng, J.-Q. Guan, H.-M. Zhang, C.-L. Song,



- L. Wang, K. He, Q.-K. Xue, and X.-C. Ma, *Phys. Rev. B* **91**, 121113 (2015).
- [82] G. Monney, C. Monney, B. Hildebrand, P. Aebi, and H. Beck, *Phys. Rev. Lett.* **114**, 086402 (2015).
- [83] K. Sugawara, Y. Nakata, R. Shimizu, P. Han, T. Hito-sugi, T. Sato, and T. Takahashi, *ACS Nano* **10**, 1341 (2015).
- [84] B. Hildebrand, T. Jaouen, C. Didiot, E. Razzoli, G. Monney, M.-L. Mottas, A. Ubaldini, H. Berger, C. Barreateau, H. Beck, D. R. Bowler, and P. Aebi, *Phys. Rev. B* **93**, 125140 (2016).
- [85] A. Novello, M. Spera, A. Scarfato, A. Ubaldini, E. Giannini, D. Bowler, and C. Renner, *Phys. Rev. Lett.* **118**, 017002 (2017).
- [86] D. Pasquier and O. V. Yazyev, *Phys. Rev. B* **98**, 235106 (2018).
- [87] Z. Jiang, Y. Li, S. Zhang, and W. Duan, *Phys. Rev. B* **98**, 081408 (2018).
- [88] C. Chen, B. Singh, H. Lin, and V. M. Pereira, *Phys. Rev. Lett.* **121**, 226602 (2018).
- [89] C. Lian, S.-J. Zhang, S.-Q. Hu, M.-X. Guan, and S. Meng, (2019), [arXiv:1901.00610 \[cond-mat.mes-hall\]](#).
- [90] H. P. Hughes, *J. Phys. C: Solid State Phys.* **10**, L319 (1977).
- [91] N. Wakabayashi, H. Smith, K. Woo, and F. Brown, *Solid State Communications* **28**, 923 (1978).
- [92] J. H. Gaby, B. DeLong, F. Brown, R. Kirby, and F. Lévy, *Solid State Communications* **39**, 1167 (1981).
- [93] K. Motizuki, N. Suzuki, Y. Yoshida, and Y. Takaoka, *Solid State Communications* **40**, 995 (1981).
- [94] N. Suzuki, A. Yamamoto, and K. Motizuki, *Solid State Communications* **49**, 1039 (1984).
- [95] J. M. Lopez-Castillo, A. Amara, S. Jandl, J.-P. Jay-Gerin, C. Ayache, and M. J. Aubin, *Phys. Rev. B* **36**, 4249 (1987).
- [96] M. Holt, P. Zschack, H. Hong, M. Y. Chou, and T.-C. Chiang, *Phys. Rev. Lett.* **86**, 3799 (2001).
- [97] A. Bussmann-Holder and A. R. Bishop, *Phys. Rev. B* **79**, 024302 (2009).
- [98] J. van Wezel, P. Nahai-Williamson, and S. S. Saxena, *Phys. Rev. B* **81**, 165109 (2010).
- [99] K. Rossnagel, *New J. Phys.* **12**, 125018 (2010).
- [100] M. Calandra and F. Mauri, *Phys. Rev. Lett.* **106**, 196406 (2011).
- [101] F. Weber, S. Rosenkranz, J.-P. Castellan, R. Osborn, G. Karapetrov, R. Hott, R. Heid, K.-P. Bohnen, and A. Alatas, *Phys. Rev. Lett.* **107**, 266401 (2011).
- [102] Z. Zhu, Y. Cheng, and U. Schwingenschlgl, *Phys. Rev. B* **85**, 245133 (2012).
- [103] V. Olevano, M. Cazzaniga, M. Ferri, L. Caramella, and G. Onida, *Phys. Rev. Lett.* **112**, 049701 (2014).
- [104] B.-T. Wang, P.-F. Liu, J.-J. Zheng, W. Yin, and F. Wang, *Phys. Rev. B* **98**, 014514 (2018).
- [105] T. Kaneko, Y. Ohta, and S. Yunoki, *Phys. Rev. B* **97**, 155131 (2018).
- [106] F. J. D. Salvo, D. E. Moncton, and J. V. Waszczak, *Phys. Rev. B* **14**, 4321 (1976).
- [107] V. Popescu and A. Zunger, *Phys. Rev. B* **85**, 085201 (2012).
- [108] See Supporting Information at URL for further discussion..
- [109] Z.-G. Fu, Z.-Y. Hu, Y. Yang, Y. Lu, F.-W. Zheng, and P. Zhang, *RSC Adv.* **6**, 76972 (2016).
- [110] Z.-G. Fu, J.-H. Wang, Y. Yang, W. Yang, L.-L. Liu, Z.-Y. Hu, and P. Zhang, *EPL* **120**, 17006 (2017).
- [111] J. J. Mortensen, L. B. Hansen, and K. W. Jacobsen, *Phys. Rev. B* **71**, 035109 (2005).
- [112] J. Enkovaara, C. Rostgaard, J. J. Mortensen, J. Chen, M. Dulak, L. Ferrighi, J. Gavnholt, C. Glinsvad, V. Haikola, H. A. Hansen, H. H. Kristoffersen, M. Kuusma, A. H. Larsen, L. Lehtovaara, M. Ljungberg, O. Lopez-Acevedo, P. G. Moses, J. Ojanen, T. Olsen, V. Petzold, N. A. Romero, J. Stausholm-Møller, M. Strange, G. A. Tritsaridis, M. Vanin, M. Walter, B. Hammer, H. Hkkinen, G. K. H. Madsen, R. M. Nieminen, J. K. Nørskov, M. Puska, T. T. Rantala, J. Schiøtz, K. S. Thygesen, and K. W. Jacobsen, *J. Phys.: Condens. Matter* **22**, 253202 (2010).
- [113] A. H. Larsen, J. J. Mortensen, J. Blomqvist, I. E. Castelli, R. Christensen, M. Dulak, J. Friis, M. N. Groves, B. Hammer, C. Hargus, E. D. Hermes, P. C. Jennings, P. B. Jensen, J. Kermode, J. R. Kitchin, E. L. Kolsbjerg, J. Kubal, K. Kaasbjerg, S. Lysgaard, J. B. Maronsson, T. Maxson, T. Olsen, L. Pastewka, A. Peterson, C. Rostgaard, J. Schiøtz, O. Schtt, M. Strange, K. S. Thygesen, T. Vegge, L. Vilhelmsen, M. Walter, Z. Zeng, and K. W. Jacobsen, *J. Phys.: Condens. Matter* **29**, 273002 (2017).
- [114] P. E. Blchl, *Phys. Rev. B* **50**, 17953 (1994).
- [115] J. P. Perdew, K. Burke, and M. Ernzerhof, *Phys. Rev. Lett.* **77**, 3865 (1996).
- [116] H. J. Monkhorst and J. D. Pack, *Phys. Rev. B* **13**, 5188 (1976).
- [117] S. Sharma, J. K. Dewhurst, A. Sanna, and E. K. U. Gross, *Phys. Rev. Lett.* **107**, 186401 (2011).
- [118] Z. Yuan and S. Gao, *Computer Physics Communications* **180**, 466 (2009).
- [119] J. Yan, K. W. Jacobsen, and K. S. Thygesen, *Phys. Rev. B* **84**, 235430 (2011).
- [120] C. Lian, S.-q. Hu, J. Zhang, C. Cheng, Z. Yuan, S. Gao, and S. Meng, [arXiv:1803.01604 \[cond-mat.mtrl-sci\]](#).